Anterior Segment Anatomy and Conventional Outflow Physiology of the Tree Shrew (*Tupaia belangeri*)

Jessica V. Jasien,[1] A. Thomas Read,[2] Joseph van Batenburg-Sherwood,[3] Kristin M. Perkumas,[4] C. Ross Ethier,[2] W. Daniel Stamer,[4] and Brian C. Samuels[5]

[1]Vision Science Graduate Program, School of Optometry, University of Alabama at Birmingham, Birmingham, Alabama, United States
[2]Coulter Department of Biomedical Engineering, Georgia Institute of Technology and Emory University, Atlanta, Georgia, United States
[3]Department of Bioengineering, Imperial College London, London, United Kingdom
[4]Department of Ophthalmology, Duke University, Durham, North Carolina, United States
[5]Department of Ophthalmology and Visual Sciences, School of Medicine, University of Alabama at Birmingham, Birmingham, Alabama, United States

Correspondence: Brian C. Samuels, Department of Ophthalmology and Visual Sciences, The University of Alabama at Birmingham School of Medicine, 1720 University Blvd, Birmingham, AL 35294, USA; bsamuels@uab.edu.

Received: January 14, 2021
Accepted: October 26, 2021
Published: January 18, 2022

Citation: Jasien JV, Read AT, van Batenburg-Sherwood J, et al. Anterior segment anatomy and conventional outflow physiology of the Tree Shrew (*Tupaia belangeri*). *Invest Ophthalmol Vis Sci.* 2022;63(1):21. https://doi.org/10.1167/iovs.63.1.21

Purpose. Rodent and primate models are commonly used in glaucoma research; however, both have their limitations. The tree shrew (*Tupaia belangeri*) is an emerging animal model for glaucoma research owing in part to having a human-like optic nerve head anatomy, specifically a collagenous load-bearing lamina. However, the anterior segment anatomy and function have not been extensively studied in the tree shrew. Thus, the purpose of this study was to provide the first detailed examination of the anterior segment anatomy and aqueous outflow facility in the tree shrew.

Methods. Aqueous outflow dynamics were measured in five ostensibly normal eyes from three tree shrews using the iPerfusion system over a range of pressures. Gross histological assessment and immunohistochemistry were performed to characterize anterior segment anatomy and to localize several key molecules related to aqueous outflow.

Results. Anterior segment anatomy in tree shrews is similar to humans, demonstrating a scleral spur, a multilayered trabecular meshwork and a circular Schlemm's canal with a single lumen. Average outflow facility was 0.193 µL/min/mm Hg (95% confidence interval, 0.153–0.244), and was stable over time. Outflow facility was more similar between contralateral eyes (approximately 5% average difference) than between eyes of different animals. No significant dependence of outflow facility on time or pressure was detected (pressure–flow nonlinearity parameter of 0.01 (95% % confidence interval, −0.29 to 0.31 CI µL/min/mm Hg).

Conclusions. These studies lend support to the usefulness of the tree shrew as a novel animal model in anterior segment glaucoma and pharmacology research. The tree shrew's cost, load-bearing collagenous lamina cribrosa, and lack of washout or anterior chamber deepening provides a distinct experimental and anatomic advantage over the current rodent and nonhuman primate models used for translational research.

Keywords: aqueous outflow, aqueous humor facility, Tree Shrew, histology, anterior segment

An IOP is currently the only modifiable risk factor for glaucoma, and thus a robust and prolonged decreased in the IOP is the main objective of glaucoma treatments. IOP is determined by a combination of aqueous humor secretion rate (Q_{in}), drainage rate through the unconventional pathway (Q_u), outflow facility (C) of the conventional pathway (trabecular meshwork [TM], Schlemm's canal [SC] and distal vessels), and episcleral venous pressure (P_e). This relationship is summarized in the modified Goldmann's equation.[1] In open-angle glaucoma, an elevated IOP is caused by a reduced conventional outflow facility.[2–4] Because IOP lowering is the mainstay of glaucoma treatment, it is important to understand the effect of ocular medications on the various factors that govern IOP. Although most current treatments target the reduction of aqueous production (Q_{in})[5–7] or enhance unconventional outflow (Q_u),[8] newer treatments now target and improve conventional outflow function (C).[9] Even with the variety of medications currently available, treatments often do not achieve "target IOP" for patients, and thus there continues to be a critical unmet need for additional pharmacological agents to treat glaucoma.

Before initiating clinical trials, ocular medications are tested in pre-clinical animal models. Rodents, rabbits, dogs, and nonhuman primates (NHP) are the most commonly used animals in glaucoma studies; however, all have their limitations, and thus developing additional nonprimate

animal models that more accurately resemble the anatomy and aqueous humor dynamics of humans is desired. Although anatomically similar to humans, NHPs are not necessarily the ideal model. In addition to cost and growing ethical concerns, outflow facility increases over time during perfusion in NHP eyes. This increase in outflow facility over time, also known as washout, is not seen in humans.[10–16] Another frequently used animal model of glaucoma is the rodent. In addition to lacking the wash out phenomenon seen in NHPs and other animals, rodents have the advantage of targeted genetic manipulations. However, rodent eyes, particularly those of mice, are small with very low outflow rates and it therefore becomes technically challenging to measure facility with repeatability and accuracy in these animals.

The tree shrew (*Tupaia belangeri*) is closely related to primates.[17] They have been used for years as an induced experimental myopia model[18–20] and have been validated recently as an animal model for glaucoma research based on the posterior segment anatomy.[17] Compared with NHPs, tree shrews are less costly and with the advent of CRISPR technology, genetic manipulations are feasible to facilitate an understanding of the genetic basis of diseases, such as glaucoma. However, to date, the anterior segment anatomy and aqueous outflow facility of the tree shrew have not been studied systematically.

We hypothesize that the anatomy of the aqueous outflow pathways in the tree shrew will be similar to those in human and that the tree shrew's outflow facility will lie between those of rodents and NHP.[10–12,21–26] We have adapted the iPerfusion system, originally purpose built to provide very accurate measures of outflow facility in a wide variety of small animals,[26,27] to measure outflow facility in the tree shrew. We also undertake the first systematic characterization of the morphology of the tree shrew conventional outflow pathway.

Methods

Animals

All animals were handled in accordance with the ARVO Statement for the Use of Animals in Ophthalmic and Vision Research under an approved Institutional Animal Care and Use Committee protocol monitored by the University of Alabama at Birmingham (UAB). Five eyes from three tree shrews (*Tupaia belangeri*), including two paired sets of eyes, were used (Table 1). Two males and one female, each approximately 22 months old, with no known ocular abnormalities were used for this study (Table 1). For reference, tree shrews reach sexual maturity at approximately 3 months of age; thus, these animals are approaching middle age. Animals were housed individually on a 12-hour light–dark cycle, and had access to food and water ad libitum. Euthanization was carried out with an overdose of xylazine (50 mg i.p.) and eyes were carefully enucleated at UAB and shipped overnight on ice to Duke University for outflow facility measurement the following morning. The time interval between enucleation and cannulation was between 17 and 24 hours, depending on the animal.

Table 1. Animal Demographics

Animal Number	Eye	Sex	Age (mo)
1669	OS	Male	22
1672	OD	Female	22
1672	OS	Female	22
1673	OD	Male	22
1673	OS	Male	22

Histology

Preparation of Whole Globes. After the perfusion experiments were completed, the eyes were perfusion fixed with 4% EM grade paraformaldehyde for 30 minutes at 8 mm Hg. Eyes were then removed from the custom perfusion platform and immersion fixed in 4% EM grade paraformaldehyde for an additional 30 minutes to ensure complete penetration of the globe before being stored at 4°C. Eyes were then shipped to Georgia Tech for histological analysis. To improve the infiltration of processing solutions into whole globes, small cuts were made in the sclera and cornea, and fluid was gently injected into the openings using a 25G needle. Intact eyes were cryoprotected by immersion in a sucrose (Sigma, St Louis, MO) solution, initially 15% in PBS, followed by 30% in PBS, and finally a 1:1 solution of 30% sucrose in PBS: Optimal Cutting Temperature (OCT) media (EMS). The incubations were carried out for approximately 2 hours per transition on a slow rotator. The eyes were embedded in OCT and flash-frozen by immersion in 2-methylbutane (Sigma) cooled by liquid nitrogen. It should also be noted that eyes were perfused with pilocarpine after the perfusion experiments for an ancillary perfusion. However, a lack of consistent pupil constriction caused concern that the intracameral delivery of pilocarpine may have been an issue and resulting data inaccurate; thus, these pilot pharmacological data are not shown in this study.

Immunohistochemistry. Frozen 10-µm-thick midsagittal sections were cut with a CryoStar NX70 cryostat (ThermoFisher Scientific, Waltham, MA) and collected on gelatin-coated slides. The tissue was probed with antibodies raised against myocilin, CD31, and α-smooth muscle actin. The sections were washed in PBS, permeabilized in 0.2% Triton-X 100 for 6 minutes, blocked in 10% goat serum for 30 minutes, incubated in primary antibodies for 3 hours at room temperature and fluorescent secondary antibodies for 3 hours at room temperature. The nuclei were stained with DAPI (NucBlu, ThermoFisher Scientific). Sections were mounted in Prolong Gold (ThermoFisher Scientific) and examined on a Leica DMB6 epifluorescent microscope (Leica Microsystems, Wetzlar, Germany). The primary antibodies used were a-myocilin clone #297817 from R&D Systems (Minneapolis, MN; cat# MAB3446), Abcam (Cambridge, UK; Cat# ab41552), a-myocilin N-15 from Santa Cruz (#SC-21243), an a-myocilin antibody from the Stamer lab[28,29]; a-CD31, clone JC/70A (cat#ab9498, abcam); and a-α-smooth muscle actin (Cat#ab9498, abcam). Secondary antibodies used were goat a-mouse Alexa 488, 546 and 647; and goat a-rabbit Alexa 488 and 546 (ThermoFisher Scientific).

Gross and Microscopic Anatomy. To observe the anatomical relationships among the limbal structures, sections were cut through intact whole globes. To overcome the loss of structural integrity that often occurs when preparing sections of eyeballs from larger species, a tree shrew-specific protocol was developed as a modification of that used in the Norton Laboratory at UAB,[30] based on subsequent personal communications with Dr. Norton. Briefly, after cryosections were harvested from the frozen whole globes (as described elsewhere in this article), there

remained approximately one-half to one-third of the eyeball, including the mid-sagittal region. Excess OCT was trimmed from this tissue followed by immersion in cold Karnovsky's fixative and the eye was placed on a slow rotator in a fridge overnight. Thus, as the OCT melted, fixative infiltrated the exposed tissue, preserving the structures of the limbus in place. On a slow rotator, the tissue was washed in Sorensen's buffer for 3 hours, fixed in 1% OsO_4 in buffer for 2 hours, washed, then dehydrated through an ethanol series over a 6-hour period. The samples were transitioned to propylene oxide over the next 12 hours, infiltrated in Spurr's resin over a 48-hour period, embedded in Spurr's resin for 24 hours in a vacuum desiccator, and cured in a 65°C oven overnight. Because the resin would not infiltrate the lens, the hardened blocks of tissue remained impossible to section. To overcome this obstacle, the lens was drilled out, refilled with fresh resin, and then the block was returned to the oven to cure. The tissue was sectioned on a Leica UC7 Ultramicrotome (Leica Microsystems) equipped with an 8-mm-thick glass knife. The 1- to 2-µm thick sections were stained with toluidine blue and/or polychromatic stain[31] and examined with a Leica DMB 6 microscope.

RT-PCR

Using the Trizol method (ThermoFisher Scientific), RNA was isolated from TM tissue dissected from four pairs of tree shrew eyes and three human corneal scleral rims after button removal for corneal transplant surgery. The tissue was homogenized in Trizol using a dounce tissue grinder (10 strokes). Chloroform was added for phase separation of RNA from DNA and protein, and subsequently was cleaned by two ethanol washes and centrifugation steps. RNA was reconstituted in purified water.

Taqman primers (ThermoFisher Scientific) preselected for myocilin (Hs 00165345_m1 human) and GAPDH (Hs 02758991_g1 human) were used for the human TM tissue and a custom primer was designed for tree shrew myocilin based on a corresponding location of the human primer (assay location: base pair 827, amplicon length: 86 base pairs). cDNA was synthesized using the Maxima first strand cDNA synthesis kit (ThermoFisher Scientific), which included a step to eliminate genomic DNA. The cDNA was then used in the Taqman assay system using a Biorad CX96 real time PCR machine. Controls included one sample that did not contain reverse transcriptase and another that excluded the cDNA template.

iPerfusion

As described by Sherwood et al.,[27] the iPerfusion system comprises an actuated pressure reservoir to control pressure (P), a thermal flow sensor to measure flow rate (Q), a differential pressure measurement system to measure the pressure within the eye relative to the pressure within a bath in which the eye is immersed, and an automated computerized interface for the characterization of the flow–pressure relationship. Similar to previous studies with the iPerfusion system.[26,27] Goldmann's equation was altered to include an additional component, the inflow from the perfusion system (Q), to obtain a single equation to describe aqueous humor dynamics: $Q_{in} + Q = C(IOP - P_e) + Q_u$. The configuration of the system for the perfusion of the tree shrew eyes was identical to that used for previous mouse and rat perfusions.[21,26,27,32] A Borosilicate glass micropipette was handmade using a K.T. Brown Type Micro-Pipette Beveler (Model BV-10; Sutter Instrument, Novato, CA) to shape the bevel tip with a suitable resistance for perfusion, here measured to be 0.04 mm Hg/µL/min).[26] The glass needles were mounted on a micromanipulator for cannulation of the anterior chamber (AC) of the tree shrew eyes.

Before cannulations, the system was calibrated as described previously.[27] Enucleated eyes were fixed to a custom platform, cannulated with the above-described glass needles, and submerged in a temperature-controlled (35 ± 0.5°C) PBS bath. Eyes remained submerged throughout the entire perfusion experiment. IOP was held at 8 mm Hg for 30 minutes to allow them to acclimatize before starting flow–pressure measurements, and the reference pressure for the study was taken as 8 mm Hg. Eyes were perfused with filtered (0.2 µm) Dulbecco's PBS with added 5.5 mM glucose.[26,27]

To provide a robust assessment of the tree shrew outflow facility, a protocol was created to examine time-dependent (typically associated with washout) and pressure-dependent (typically associated with AC deepening) changes in outflow facility, which occur in primate and ex vivo rodent eyes, respectively. Hence, we used a three-stage staggered protocol with pressure steps of [8, 12.5, 17], [9.5, 14, 18.5], and [11, 15.5, 20] mm Hg. This approach yielded a 1.5-mm Hg increment between individual pressure steps and allowed for the decoupling of pressure and time. For each step, the steady state was interpreted as when the rate of change of the flow rate was less than $dQ/dt = 3$ nL/min/min consistently for 1 minute. The final 300 seconds of pressure and flow data were then filtered with a 60-second Savitsky–Golay filter, and the average values were taken as the flow and pressure for each step. Using the method established previously for mice and rats, for each eye the steady state flow (Q) and pressure (P) values were fit with the model $Q = C_r\ (P/P_r)^{\beta}\ P$, where C_r is the reference facility at reference pressure P_r, defined to be 8 mm Hg for the current data. β is a nonlinearity parameter that has been found to be positive in mice, corresponding with facility increasing with pressure that is attributed to AC deepening. Note that the model assumes zero flow at zero pressure, consistent with direct measurements.

To evaluate whether the facility demonstrated time dependence, which would be associated with the washout phenomenon, we developed the following approach, which separates the effect of perfusion pressure on facility from the effect of time on facility. Using the value of β for a given eye as above, we calculated a value of the facility corrected for perfusion pressure dependence, $C_{cor,j}$, for each pressure step, j, according to $C_{cor,j} = Q_j/P_j(P_r/P_j)^{\beta}$. Random deviations of $C_{cor,j}$ from C_r can arise from experimental uncertainty, but a systematic change in $C_{cor,j}$ over time would indicate a time-dependence of outflow facility. We, therefore, plotted $C_{cor,j}$ against t_j for each eye, and used linear regression to calculate the slope, dC_{cor}/dt, in units of microliters per minute per millimeter of mercury per hour. Values of dC_{cor}/dt were compared with the null hypothesis that $dC_{cor}/dt = 0$, indicating a negligible effect of time on outflow facility.

Statistics

Statistical analyses were similar to that derived in previous studies performed on mice using the iPerfusion system.[26,27] In brief, mouse studies have shown that outflow facility

(C_r) is best represented as a lognormal distribution.[26,27] Thus, the log-transformed reference facility $Y_r = \ln(C_r)$ is normally distributed, allowing standard parametric statistical analyses.[27] Similar to mice,[21,26,27] rats,[23,32] and other species where a lognormal distribution of outflow facility is the norm,[33,34] our data in the tree shrew were also consistent with a lognormal distribution (Anderson Darling test, Y_r, $P = 0.59$) In addition, the nonlinearity values, β ,were normally distributed ($P = 0.66$). As measured, flow rate and pressure are already normally distributed, they are reported as the means ± half-width of the 95% confidence interval (CI) as previously described.[26,27]

Results

Histology

Gross and Microscopic Anatomy. Tree shrew globes (Fig. 1) measured approximately 8.5 mm in diameter, which is much smaller than humans (28 mm), but significantly larger than rats (6.4 mm) and mice (3.3 mm). Notably, the lens of the tree shrew occupied a smaller proportion of the total eye cross-sectional area compared with mice, but the lens remains a larger proportion of the tree shrew eye compared with humans. In mid sagittal sections, the area of the lens of the tree shrew comprised 24.3% ($n = 4$; stan-

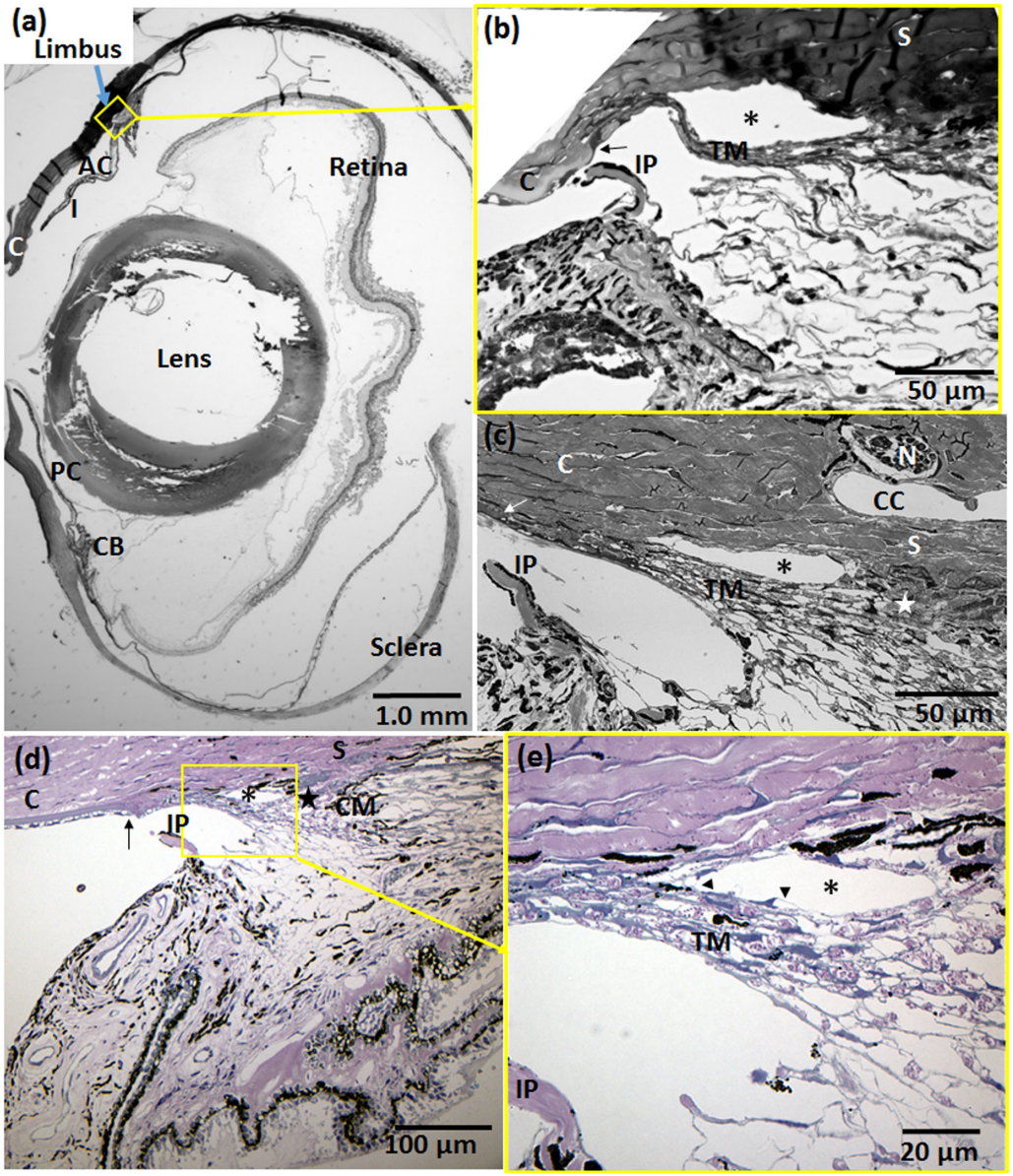

Figure 1. The eyes of three tree shrews as seen by light microscopy, illustrating gross and microscopic anatomy. (**A**) Midsagittal section through whole globe. Note detachment of retina, which occurred during processing. (**B–E**) are sagittal sections through the limbus, with (**B**) being an inset from (**A**) and (**E**) being an inset from (**D**). In (**B**) SC (*) appears dilated and TM sheets are compressed. Note intertrabecular spaces in TM of (**C**) and (**E**), giant vacuoles (arrowheads) in SC of (**E**) and a collector channel (CC) and nearby nerve (N) in (**C**). (**A–C**) Stained with toluidine blue and (**D**, **E**) stained with polychromatic stain (see methods). Panels (**A–C**) were from eyes perfused with pilocarpine (pilot pharmacological data not shown) whereas (**D**, **E**) were from eyes perfused with vehicle only. arrow, posterior terminus of Descemet's membrane; C, cornea; CB, ciliary body; CM, ciliary muscle; I, iris; IP, iridial process; N, nerve; PC, posterior chamber; S, sclera; star, scleral spur. (**A**, **B**) Images were from animal 1673 OD; (**C**) is from 1726 OD and (**D**, **E**) were from 1672 OD.

Investigative Ophthalmology & Visual Science

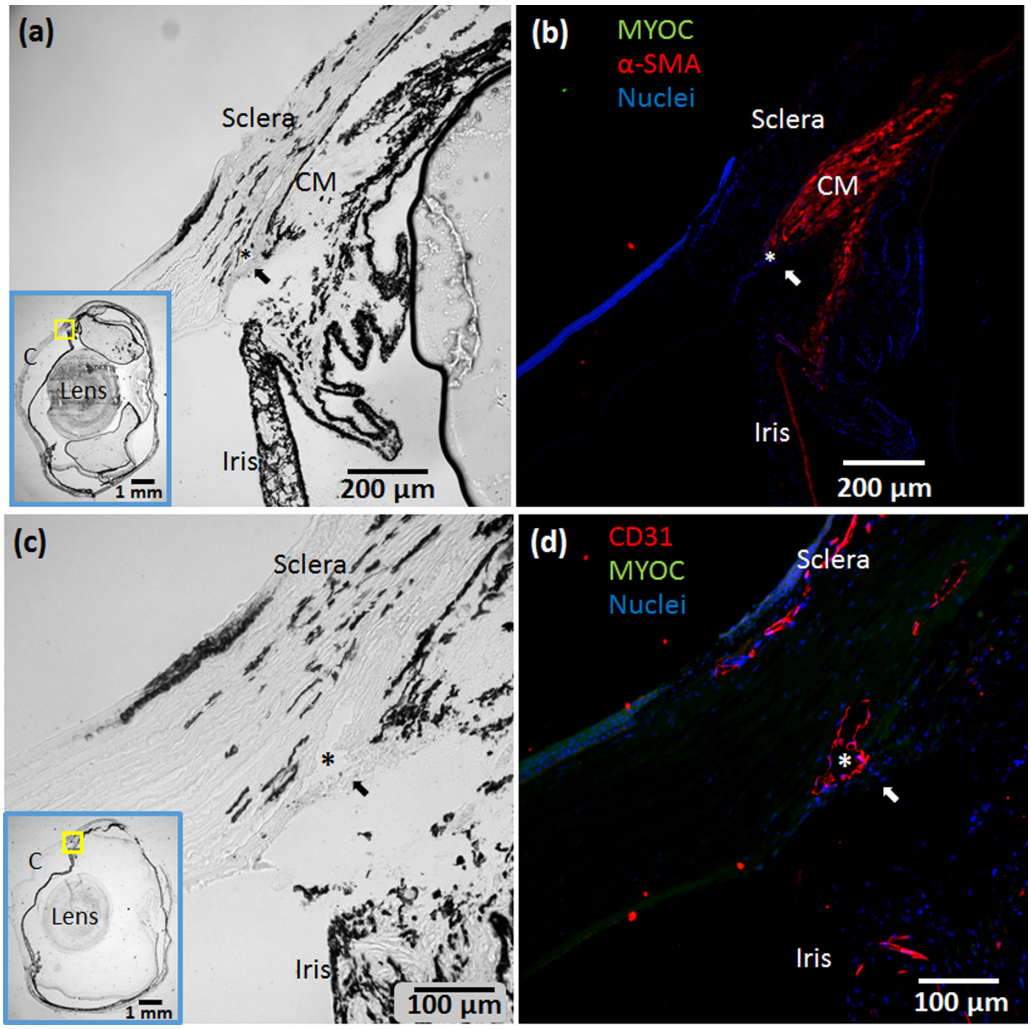

Figure 2. Immunolabelling of tree shrew eye cryosections. (**A**, **C**) An overview inset (outlined in blue with yellow box outlining the limbus) and brightfield images of corresponding fluorescent images (**B**) and (**D**) respectively. (**B**) Labelling for α-smooth muscle actin (α-SMA, red), myocilin (green, using antibody 3446 from R&D) and nuclei (blue); (**D**) was labelled for CD31 (red), myocilin (green[28,29]) and nuclei (blue). Note that α-SMA colocalizes with ciliary muscle, parts of the ciliary body, and the iris, whereas a-CD31 labels endothelial cells lining SC and blood vessels. Myocilin could not be detected with the antibodies we used. Arrow, TM; asterisk, SC; C, cornea; CM, ciliary muscle. (**A–D**) Images were from animal 1672 OS.

dard deviation [SD], ±4.7%) of the total whole globe area compared with mice in which the value was 39.0% ($n = 4$; SD ±3.5); in humans, it was 6.2% ($n = 3$; SD ±1.0) (unpublished data).

The TM was open and accessible, with an irideocorneal angle of approximately 30°. Many sections demonstrated a prominent and thick iridial process originating from the anterior iris stroma near the iris root. The processes often projected into the AC but did not appear to have attachments to the TM, scleral spur, or corneal endothelium that would block flow of aqueous through the conventional pathway. We observed a well-developed, large single-lumen SC, variable in width (range, 77–96 µm) and in height (range, 8–14 µm), with a relatively smooth inner and outer wall. In some sections a large collector channel was observed near the SC lumen. The inner and outer walls of SC were lined by a thin endothelial cell layer, with giant vacuoles observed in the inner and outer wall, as well as in the collector channels. The TM consisted of multiple interconnected sheets (approximately 7 layers), joined by thin strands, with an approximate TM thickness ranging from 16 µm anteriorly to 50 µm posteriorly. The TM contained prominent, somewhat elongated intertrabecular spaces and associated pleomorphic nuclei. Within the TM sheets, prominent clumps of dark-staining material, either isolated or surrounded by a pale-staining material, were present. At various locations in the limbal region (near the collector channels, ciliary body, and TM), small nerves containing several myelinated axons were seen. We also observed very prominent, scattered, large (≤20 µm in length), densely packed, elongated clumps of pigment. The scleral spur was situated posterior to SC and the TM with fibers of the ciliary muscle inserting into it. Descemet's membrane was observed as a thin homogeneous layer approximately 6 µm thick extending posteriorly and terminating at the anterior apex of the TM.

Immunohistochemistry. Immunolabelling demonstrated the presence of two key proteins in the limbus (Fig. 2). Specifically, anti–α-smooth muscle actin strongly labelled a region consistent with the ciliary muscle, and weakly with the posterior epithelium of the iris, but not

Investigative Ophthalmology & Visual Science

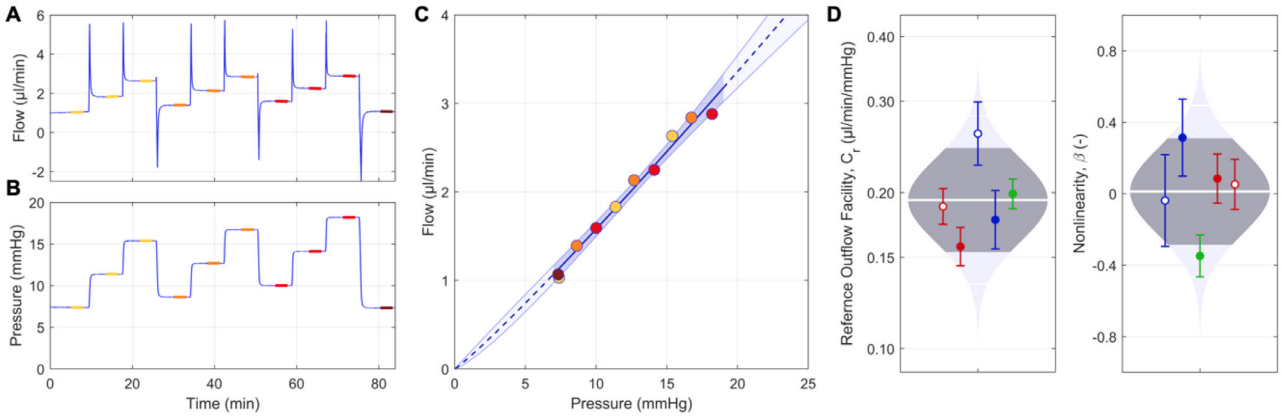

Figure 3. (**A**) Flow and (**B**) pressure traces from eye 1672 OD. (**C**) Flow–pressure plot from eye 1672 OD shown with power law fit (line) and 95% CI (shaded region). (**D**) Cello plot of the reference facility, C_r, (left) and the nonlinearity parameter, β, (right) for all studied eyes. The error bars show 95% margin of error and the grey band is the 95% CI from the regression fit. The shaded regions show the best estimates of the sample distributions. The geometric mean and two-sigma are shown by the white horizontal lines, and the dark central areas show the 95% CI of the mean values of the reference outflow facility (*left*) and nonlinearity parameter (*right*) of all eyes, where each color represents an animal and each eye.

extending into the TM. In addition, anti-CD31 intensely labelled both the inner and outer endothelia of SC, as well as cells lining lumens (likely blood vessels) scattered throughout the sclera and episcleral/conjunctiva. In contrast, myocilin could not be detected in any of the tree shrew samples, despite using four different antimyocilin antibodies.

RT-PCR

Owing to the unavailability of antibodies that cross-react with tree shrew myocilin, we performed real-time PCR of RNA isolated from TM tissue dissected from tree shrew eyes. As a control, we compared expression levels to RNA isolated from TM tissue from human donor eyes. As reported previously (PMID: 10509652), we observed high expression levels of myocilin in TM from human eyes (cycle threshold value of 19.9, compared with 21.32 for GAPDH). Similarly, we observed high expression levels of myocilin in TM of tree shrew (cycle threshold of 21.68 for myocilin compared with cycle threshold of 25.11 for GAPDH), suggesting an important role for myocilin in tree shrew TM biology.

Aqueous Outflow Facility

Representative flow and pressure traces are seen in Figures 3A, 3B, with stagger stage color coding corresponding with individual flow–pressure points in Figure 3C. The flow–pressure relationship was essentially linear (Fig. 3C) for all eyes, with an average value of the nonlinearity parameter, β, of 0.01 µL/min/mm Hg (95% CI, −0.29 to 0.31; 2SD range, −0.47 to 0.49) over all eyes. Using a single sample t test, this value was found to be not significantly different from zero ($P = 0.91$). All reference outflow facilities and nonlinearity parameters are shown in Figure 3D and summarized in Table 2. The mean outflow facility was 0.19 µL/min/mm Hg (95% CI, 0.15–0.24; 2SD range, 0.13–0.28). The average rate of change in pressure-corrected facility versus perfusion time, dC_{cor}/dt, was 0.00003 µL/min/mm Hg (95% CI, −0.019 to 0.019; @SD range, −0.03 to 0.30), which was not statistically different from zero ($P = 0.9969$) (Fig. 4). The CIs indicate that we would have been able to detect a time dependence of facility greater than approximately ±10% per hour, and we thus infer that there was no significant washout effect in the cohort of tree shrew eyes examined in this study (Fig. 4).

Discussion

These studies are the first to systematically analyze the anterior segment anatomy and outflow physiology in the tree shrew eye. Critical among these findings are that (1) the tree shrew anatomy is similar to humans with a multilayered trabecular structure and a scleral spur, (2) the outflow facility was measured in a range between rodent and NHP outflow facility, (3) there is either very little or no washout during perfusion studies, and (4) the flow–pressure relationship is essentially linear. These results provide strong proof of concept for future studies aimed at investigating glaucoma pharmacology in the tree shrew and additional outflow physiology studies. It is possible that the tree shrew will provide significant advantages over the models currently used. In particular, the greater outflow facility means that flow rates are larger (at a given IOP), making experimental measurements easier as compared with rodents. Further, the larger AC facilitates cannulation, and the apparent absence of AC deepening makes the interpretation of ex vivo facility measurements much easier.

Related to the latter point, we found that the parameter, β, which quantifies the nonlinearity of the pressure–flow

Table 2. Analysis of Five Eyes of Three Tree Shrew Outflow Facility

	Mean	Lower CI	Upper CI	Lower 2SD	Upper 2SD
Facility (µL/min/mm Hg)	0.193	0.153	0.244	0.133	0.281
Nonlinearity	0.01	−0.29	0.31	−0.47	0.49

Investigative Ophthalmology & Visual Science

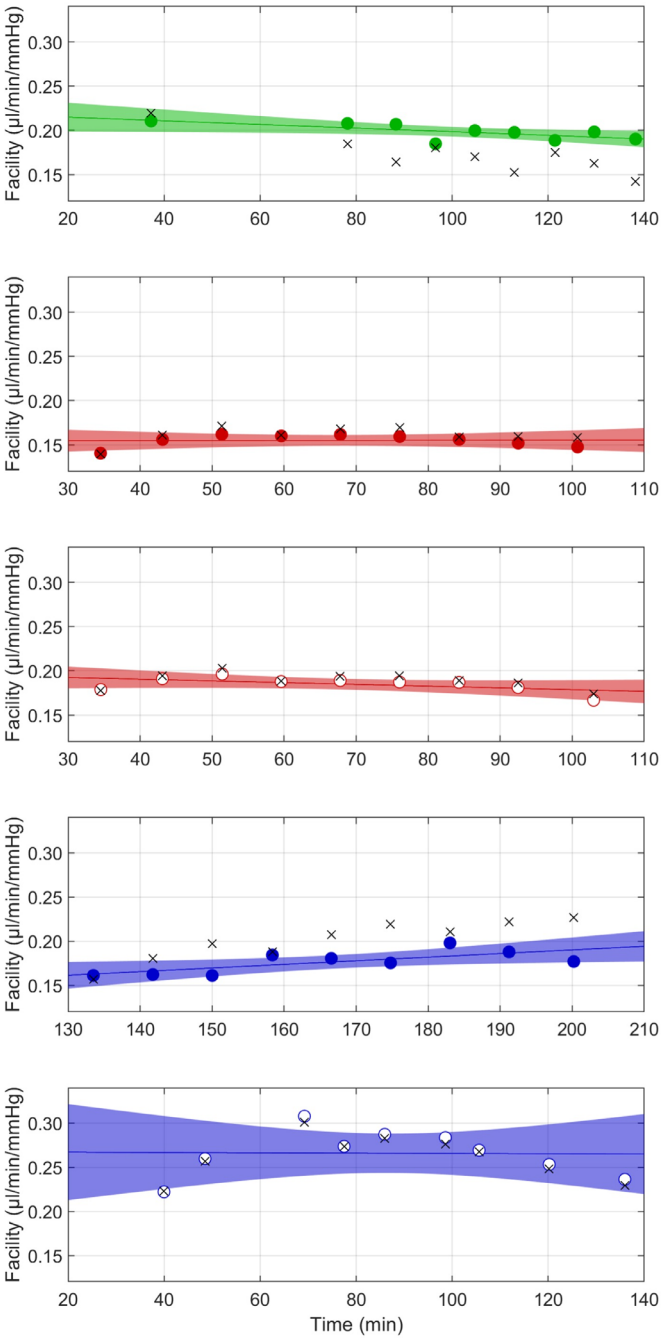

Figure 4. Plots of pressure-corrected outflow facility, $C_{j,cor}$, against time, t_j, for each of the five eyes (marker color corresponds with Fig. 3D). Crosses (x) indicate uncorrected facility values given by Q_j/P_j. Lines show linear fits with shaded areas indicating 95% confidence bounds to the fit.

relationship (and hence the pressure dependence of the outflow facility) (Fig. 3D), was not significantly different from zero ($P = 0.91$) (mean, 0.01 µL/min/mm Hg; 95% CI, −0.29 to 0.31; 2 SD range, −0.47 to 0.49), which implies that either there was no deepening of the AC at the perfusion pressures tested, or that any deepening of the AC did not affect the outflow facility. Previous studies in mice have shown a significant nonlinearity (positive β) that corresponds with AC deepening and an increase in outflow facility with increasing pressure.[21,26,27] The linearity of the pressure–flow relationship is an important benefit of the tree shrew, because deepening owing to the placement of a needle in the AC of rodents affects outflow dynamics[35] and is, thus, a potential confounding factor in ex vivo perfusion studies. Future studies in the tree shrew will incorporate anterior segment OCT imaging to ascertain the extent of AC deepening during perfusions.

Grossly, the TM is multilayered and increases in thickness as one moves anteriorly to posteriorly. There is variable pigmentation; however, it is not as well-organized as the human TM, where there are distinct anterior nonpigmented and posterior pigmented regions that are thought to represent nonfiltering and filtering regions, respectively. The darkly stained material within the TM sheets may

Investigative Ophthalmology & Visual Science

actually represent fine tropocollagen filaments surrounded by the more lightly staining collagen filaments as described by Hogan et al.[36] in human TM. Future transmission electron microscopy studies on the tree shrew TM will be beneficial in elucidating this further.

Immunohistochemistry results were somewhat surprising in that, despite the use of four antimyocilin antibodies, myocilin was undetectable in the tree shrew TM. However, the RT-PCR of RNA isolated from the TM tissue of the tree shrew results showed high expression levels of myocilin in tree shrew TM. Interestingly, the Chinese tree shrew myocilin gene has been identified[37] and the protein sequence shows a 92% positive and 84% identical homology to the human sequence. Future studies should focus on identifying Northern tree shrew myocilin through the creation of a tree shrew-specific myocilin antibody and/or confirmation of myocilin expression through RNA sequencing analysis.

The SC and the downstream collector channels are also quite similar to those in the human and appear to be larger and more well developed than in the rodent.[38] Anatomically, the SC consists of a single lumen that appeared continuous in the histological sections that we observed. In addition, there was evidence of nearby collector channels that coursed through the sclera, which presumably connected with aqueous veins/intrascleral venous plexus and then episcleral veins. The presence of giant vacuoles in the endothelia of SC and the collector channels (not shown) is encouraging from a physiological standpoint; however, we were unable to confirm in this study whether the giant vacuoles were more prominent near collector channels as is seen in humans.[39] The walls of SC did stain positively for the endothelial cell marker CD-31 as expected.

From a physiological standpoint, there is a wide range in outflow facilities among various species.[2,10–12,15,16,21,23–25] Although a comprehensive assessment has never been conducted, smaller eyes tend to have a lower outflow facility. As indicated, the tree shrew eye is significantly larger than a mouse eye and moderately larger than a rat eye, with the lens taking up a much smaller proportion of the posterior segment compared with either rodent. However, the tree shrew eye is still much smaller than the eyes of most NHPs. The mean outflow facility of the five eyes in this study was 0.193 µL/min/mm Hg (95% CI, 0.153–0.244), which is comparable to the outflow facility reported by Stockslager et al.[40] of 0.085 ± 0.033 µL/min/mm Hg and 0.303 ± 0.098 µL/min/mm Hg in two different tree shrews. As predicted, this is less than the facility in NHP and humans; for example, the outflow facilities of rhesus macaques and cynomolgus NHPs have been reported to be 0.13 to 0.69 µL/min/mm Hg[24,41] and 0.46 ± 0.17 µL/min/mm Hg,[42] respectively. In addition, the tree shrew facility is greater than that of mice measured with the iPerfusion system, which average approximately 0.004 µL/min/mm Hg.[22,25–27,43,44]

Previous studies have shown multiple animal species, including the cow, cat, dog, NHP, pig, rabbit, and guinea pig eyes[11,23,25,44–60] exhibit washout during ex vivo perfusion studies, whereas this has not been reported in mouse, rat, or human eyes.[61,62] Our data indicate that tree shrews demonstrate either no washout or very low levels of washout that are below our limits of detection (<10%/h). The reason for this washout phenomenon remains unclear, but may be related to anatomical differences in how the juxtacanalicular region of the TM is anchored to SC and its basal lamina. Specifically, it has been found that the inner wall endothelial cells and juxtacanalicular connective tissue of human eyes have a more complex array of elastic fiber connections than in other animals.[63] This strong connectivity may better withstand the dynamic forces imposed during perfusion than eyes with weaker connections.[63] Future studies will examine the elastic fiber connections of the tree shrew TM–SC junction. Regardless, the data presented herein show the tree shrew exhibits either an absence or extremely low levels of washout (<10%/h); making it an attractive model to explore pharmacological studies testing novel glaucoma medications.

Previous attempts to induce ocular hypertension in the tree shrew raised questions about the angle anatomy.[17] Before using magnetic microspheres to increase the IOP, attempts were made to use laser photoablation of the TM similar to the technique used for inducing glaucoma in primates.[64–67] Gonioscopic identification of the tree shrew TM was difficult owing to what was thought to be a prominent iris root vessel. These studies indicate that prominent iris processes may have also obscured the view. Interestingly, histological analysis shows an angle that is quite similar to humans, absent of iris root vessels.

The study presented here is not without limitations. First, the study included only a small number of animals and eyes. However, the consistent outflow facility of the five eyes of the three animals is promising and provides motivation for a more thorough study with a greater number of animals and eyes. Second, the length of time from enucleation to perfusion was 17 to 24 hours. Although this was a necessity owing to the tree shrew colony being located at a different institution than where the iPerfusion system was located, this timing is similar to other outflow facility studies in other species, including humans. Further, mouse studies have shown a marginal effect on outflow facility when there is a 24-hour delay between euthanasia and eye perfusion.[22] In the future, studies will be designed such that both are in the same location and we will be able to confirm the results reported herein.

In summary, the tree shrew AC is anatomically similar to the human, with a scleral spur, a well-developed TM, and a defined outflow collector channel system. Physiologically, the tree shrew also offers significant advantages over current NHP and rodent animal models for outflow facility studies, and may be an excellent model for pharmacological studies. Given the larger size of the tree shrew eye, stability of the AC during perfusion, and lack of washout ex vivo, in vivo perfusion studies using the iPerfusion system have a high likelihood for success and will be tested in the near future. The results of this study support further investigation into the use of tree shrews in outflow facility studies, including experiments with pharmacological agents aimed at treating glaucoma.

Acknowledgments

The authors thank Iris Navarro for her time and training on the *iPerfusion* system for this study.

Supported by NIH/NEI grants R01 EY027759, EY030071, EY031710, EY028608 and EY022359, P30 EY003039, and both an unrestricted grant from Research to Prevent Blindness (RPB) to UAB as well as an RPB Physician-Scientist Award (Samuels).

Disclosure: **J.V. Jasien,** None; **A.T. Read,** None; **J. van Batenburg-Sherwood,** None; **K.M. Perkumas,** None; **C.R. Ethier,** None; **W.D. Stamer,** None; **B.C. Samuels,** None

References

1. Alm A. Uveoscleral outflow. *Eye*. 2000;14:488–491.
2. Ellingsen B, Grant W. The relationship of pressure andaqueous outflow in enucleated human eyes. *Invest Ophthalmol*. 1971;10:430–437.
3. Grant WM. Clinical measurements of aqueous outflow. *AMA Arch Ophthalmol*. 1951;46:113–131.
4. Stamer WD, Acott TS. Current understanding of conventional outflow dysfunction in glaucoma. *Curr Opin Ophthalmol*. 2012;23:135–143.
5. Yablonski M, ZImmerman T, Waltman S, Becker B. A fluorophotometric study of the effect of topical timolol on aqueous humor dynamics. *Exp Eye Res*. 1978;27:135–142.
6. Gharagozloo N, Relf S, Brubaker R. Aqueous flow is reduced by the alpha-adrenergic agonist, apraclonidine hydrochloride. *Ophthalmology*. 1988;95:1217–1220.
7. Topper J, Brubaker R. Effects of timolol, epinephrine, and acetazolamide on aqueous flow during sleep. *Invest Ophthalmol Vis Sci*. 1985;26:1315–1319.
8. Toris C, Camras C, Yablonski M. Effects of PhXA41, anew prostaglandin F2 alpha analog, on aqueous humor dynamics in human eyes. *Ophthalmology*. 1993;100:1297–1304.
9. Tanna AP, Johnson M. Rho kinase inhibitors as a novel treatment for glaucoma and ocular hypertension. *Ophthalmology*. 2018;125:1741–1756.
10. Barany E. Simultaneous measurement of changing intraocular pressure and outflow facility in the vervet monkey by constant pressure infusion. *Invest Ophthalmol*. 1964;3:135–143.
11. Erickson K, Kaufman P. Comparative effects of three ocular perfusates on outflow facility in the cynomolgus monkey. *Curr Eye Res*. 1981;1:211–216.
12. Kaufman P, True-Gabelt B, Erickson-Lamy K. Time-dependence of perfusion outflow facility in the cynomolgus monkey. *Curr Eye Res*. 1988;7:721–726.
13. Kee C, Gabelt B, Gange S, Kaufman P. Serum effects on aqueous outflow during anterior chamber perfusion in monkeys. *Invest Ophthalmol Vis Sci*. 1996;37:1840–1848.
14. Kiland J, Peterson J, Gabelt B, Kaufman P. Effect of DMSO and exchange volume on outflow resistance washout and response to pilocarpine during anterior chamber perfusion in monkeys. *Curr Eye Res*. 1997;16:1215–1220.
15. Erickson-Lamy K, Schroeder A, Bassett-Chu S, Epstein D. Absence of time-dependent facility increase ("washout") in the perfused enucleated human eye. *Invest Ophthalmol Vis Sci*. 1990;31:2384–2388.
16. Grant W. Experimental aqueous perfusion in enucleated human eyes. *Arch Ophthalmol*. 1963;69:783–801.
17. Samuels BC, Siegwart JT, Zhan W, et al. A novel Tree Shrew (Tupaia belangeri) model of glaucoma. *Invest Ophthalmol Vis Sci*. 2018;59:3136–3143.
18. Norton TT. Experimental myopia in tree shrews. *Ciba Found Symp*. 1990;155:178–194; discussion 194.
19. McBrien N, Norton T. The development of experimental myopia and ocular component dimensions in monocularly lid-sutured tree shrews (Tupaia belangeri). *Vision Res*. 1992;32:843–852.
20. Baldivia S, Levy A, Hegde S, et al. A novel organ culture model to quantify collagen remodeling in Tree Shrew sclera. *PLoS One*. 2016;11:e0166644.
21. Boussommier-Calleja A, Li G, Wilson A, et al. Physical factors affecting outflow facility measurements in mice. *Invest Ophthalmol Vis Sci*. 2015;56:8331–8339.
22. Boussommier-Calleja A, Bertrand J, Woodward D, et al. Pharmacologic manipulation of conventional outflow facility in ex vivo mouse eyes. *Invest Ophthalmol Vis Sci*. 2012;53:5838–5845.
23. Ficarrotta KR, Bello SA, Mohamed YH, Passaglia CL. Aqueous humor dynamics of the Brown-Norway rat. *Invest Ophthalmol Vis Sci*. 2018;59:2529–2537.
24. Kiland JA, Gabelt BAT, Kaufman PL. Relationship of aqueous outflow resistance to age and total volume perfused in Rhesus and Cynomolgus monkeys. *Invest Ophthalmol Vis Sci*. 2011;52:6820–6824.</.
25. Lei Y, Overby D, Boussommier-Calleja A, Stamer W, Ethier C. Outflow physiology of the mouse eye: pressure dependence and washout. *Invest Ophthalmol Vis Sci*. 2011;52:1865–1871.
26. Madekurozwa M, Reina-Torres E, Overby DR, Sherwood JM. Direct measurement of pressure-independent aqueous humour flow using iPerfusion. *Exp Eye Res*. 2017;162:129–138.
27. Sherwood JM, Reina-Torres E, Bertrand JA, Rowe B, Overby DR. Measurement of outflow facility using iPerfusion. *PLoS One*. 2016;11:e0150694.
28. Stamer WD, Perkumas KM, Hoffman EA, et al. Isolation, culture, and characterization of endothelial cells from Schlemm's canal. *Invest Ophthalmol Vis Sci*. 1998;83:1386–1395.
29. Stamer WD, Perkumas KM, Hoffman EA, et al. Coiled–coil targeting of myocilin to intracellular membranes. *Exp Eye Res*. 2006;83:1386–1395.
30. Kang R. *A light and electromicroscopic study of tree shrew sclera during normal development, induced myopia, and recovery*. [PhD thesis]. Birmingham, AL: University of Alabama at Birmingham; 1994.
31. Morikawa S, Sato A, Ezaki T. A simple, one-step polychromatic staining method for epoxy-embedded semithin tissue sections. *Microscopy (Oxf)*. 2018;67:331–344.
32. Feola AJ, Sherwood JM, Pardue MT, Overby DR, Ethier CR. Age and menopause effects on ocular compliance and aqueous outflow. *Invest Ophthalmol Vis Sci*. 2020;61:16.
33. Limpert E, Stahel WA. Problems with using the normal distribution–and ways to improve quality and efficiency of data analysis. *PLoS One*. 2011;6:e21403.
34. Limpert E, Stahel W, Abbt M. Log-normal Distributions across the sciences: keys and clues. *BioScience*. 2001;51:341–352.
35. Dijkstra B, Ruijter J, Hoyng P. Outflow characteristics of isolated anterior segments of human eyes. *Invest Ophthalmol Vis Sci*. 1996;37:2015–2021.
36. Hogan M, Alvarado J, Weddell J. *Histology of the human eye; an atlas and textbook*. Philadelphia: Saunders; 1971:xiii.
37. ncbi.nim.nih.gov. MYOC myocilin [Tupaia chinensis (Chinese tree shrew)]. Available at: https://www.ncbi.nlm.nih.gov/gene/102476403; 2019:Gene ID: 102476403. Accessed XXXX.
38. Li G, Lee C, Agrahari V, et al. In vivo measurement of trabecular meshwork stiffness in a corticosteroid-induced ocular hypertensive mouse model. *Proc Natl Acad Sci USA*. 2019;116:1714–1722.
39. Parc C, Johnson D, Brilakis H. Giant vacuoles are found preferentially near collector channels. *Invest Ophthalmol Vis Sci*. 2000;41:2984–2990.
40. Stockslager MA, Samuels BC, Allingham RR, et al. System for rapid, precise modulation of intraocular pressure, toward minimally-invasive in vivo measurement of intracranial pressure. *PLoS One*. 2016;11:e0147020.
41. Gabelt B, Crawford K, Kaufman P. Outflow facility and its response to pilocarpine decline in aging rhesus monkeys. *Arch Ophthalmol*. 1991;109:879–882.
42. Toris C, Zhan G, Wang Y, et al. Aqueous humor dynamics in monkeys with laser-induced glaucoma. *J Ocul Pharmacol Ther*. 2000;16:19–27.

43. Honjo M, Inatani M, Kido N, et al. Effects of protein kinase inhibitor, HA1077, on intraocular pressure and outflow facility in rabbit eyes. *Arch Ophthalmol*. 2001;119:1171–1178.
44. Ruben J, Moses R, Grodzki W. Perfusion outflow facility in the rabbit eye. Stabilization by EACA. *Invest Ophthalmol Vis Sci*. 1985;26:153–158.
45. Barany E. Simultaneous measurement of changing intraocular pressure and outflow facility in the Vervet monkey by constant pressure infusion. *Invest Ophthalmol Vis Sci*. 1964;31:135–143.
46. Barany E. The mode of action of pilocarpine on outflow resistance in the eye of a primate (Cercopithecusethiops). *Invest Ophthalmol Vis Sci*. 1962;1:712–727.
47. Epstein D, Patterson M, Rivers S, Anderson P. N-ethylmaleimide increases the facility of aqueous outflow of excised monkey and calf eyes. *Invest Ophthalmol Vis Sci*. 1982;22:752–756.
48. Kaufman PL, True-Gabelt B, Erickson-Lamy KA. Time-dependence of perfusion outflow facility in the cynomolgus monkey. *Curr Eye Res*. 1988;7:721–726.
49. Erickson-Lamy K, Rohen J, Grant W. Outflow facility studies in the perfused bovine aqueous outflow pathways. *Curr Eye Res*. 1988;7:799–807.
50. Fourman S, Fourman M. Correlation of tonography and constant pressure perfusion measurements of outflow facility in the rabbit. *Curr Eye Res*. 1989;8:963–969.
51. Gaasterland D, Kupfer C, Milton R, et al. Studies of aqueous humour dynamics in man. VI. Effect of age upon parameters of intraocular pressure in normal human eyes. *Exp Eye Res*. 1978;26:651–656.
52. Gaasterland D, Pederson J, MacLellan H, Reddy V. Rhesus monkey aqueous humor composition and a primate ocular perfusate. *Invest Ophthalmol Vis Sci*. 1979;18:1139–1150.
53. Gaasterland D, Pederson J, MacLellan H. Perfusate effects upon resistance to aqueous humor outflow in the rhesus monkey eye. A comparison of glutathione-bicarbonate Ringer's solution to pooled aqueous humor as perfusate. *Invest Ophthalmol Vis Sci*. 1978;17:391–397.
54. Hashimoto J, Epstein D. Influence of intraocular pressure on aqueous outflow facility in enucleated eyes of different mammals. *Invest Ophthalmol Vis Sci*. 1980;19:1483–1489.
55. Peterson W, Jocson V. Hyaluronidase effects on aqueous outflow resistance. Quantitative and localizing studies in the rhesus monkey eye. *Am J Ophthalmol*. 1974;77:573–577.
56. Melton C, DeVille W. Perfusion studies on the eyes from four species. *Am J Ophthalmol*. 1960;50:302–308.
57. Overby D, Gong H, Qiu G, Freddo T, Johnson M. The mechanism of increasing outflow facility during washout in the bovine eye. *Invest Ophthalmol Vis Sci*. 2002;43:3455–3464.
58. Rao P, Deng P, Kumar J, Epstein D. Modulation of aqueous humor outflow facility by the Rho kinase-specific inhibitor Y-27632. *Invest Ophthalmol Vis Sci*. 2001;42:1029–1037.
59. Van Buskirk E, Brett J. The canine eye: in vitro studies of the intraocular pressure and facility of aqueous outflow. *Invest Ophthalmol Vis Sci*. 1978;17:373–377.
60. Yan D, Trope G, Ethier C, Menon I, Wakeham A. Effects of hydrogen peroxide-induced oxidative damage on outflow facility and washout in pig eyes. *Invest Ophthalmol Vis Sci*. 1991;32:2515–2520.
61. Erickson-Lamy KS, AM, Bassett-Chu S, Epstein DL. Absence of time-dependent facility increase ("washout") in the perfused enucleated human eye. *Invest Ophthalmol Vis Sci*. 1990;31:2384–2388.
62. Scott P, Overby D, Freddo T, Gong H. Comparative studies between species that do and do not exhibit the washout effect. *Exp Eye Res*. 2007;84:435–443.
63. Gong H, Freddo TF. The washout phenomenon in aqueous outflow–why does it matter? *Exp Eye Res*. 2009;88:729–737.
64. Fortune B, Burgoyne CF, Cull GA, Reynaud J, Wang L. Structural and functional abnormalities of retinal ganglion cells measured in vivo at the onset of optic nerve head surface change in experimental glaucoma. *Invest Ophthalmol Vis Sci*. 2012;53:3939–3950.
65. Fortune B, Burgoyne CF, Cull G, Reynaud J, Wang L. Onset and progression of peripapillary retinal nerve fiber layer (RNFL) retardance changes occur earlier than RNFL thickness changes in experimental glaucoma. *Invest Ophthalmol Vis Sci*. 2013;54:5653–5661.
66. Burgoyne CF. The non-human primate experimental glaucoma model. *Exp Eye Res*. 2015;141:57–73.
67. Weber AJ, Kaufman PL, Hubbard WC. Morphology of single ganglion cells in the glaucomatous primate retina. *Invest Ophthalmol Vis Sci*. 1998;39:2304–2320.

Investigative Ophthalmology & Visual Science